Sea Level on the U.S. East Coast: Decadal Variability Caused by Open Ocean Wind-Curl Forcing

B. G. HONG, W. STURGES, AND ALLAN J. CLARKE

Department of Oceanography, The Florida State University, Tallahassee, Florida

(Manuscript received 18 June 1998, in final form 12 October 1999)

ABSTRACT

One of the puzzling features of sea level on the east coast of the United States is the decedal-scale variability; the fluctuations are 10–15 cm, peak to peak, at periods longer than a few years. The authors find that this variability, in the frequency band treated with the model, is largely caused by a deep-sea signal generated by the wind stress curl over the North Atlantic. A simple forced long Rossby wave model of the response of the thermocline to wind forcing is used, computing long-wave speeds from observed hydrographic data. The authors model the response of the ocean at periods longer than 3 years for the full width of the Atlantic and for the north–south extent of the main anticyclonic gyre, 18°–38°N. The model output in deep water shows remarkably good agreement with tide gauges, both at Bermuda (32°N) and Puerto Rico (18°N), as well as with dynamic height fluctuations of ~20 cm peak to peak.

Once these fluctuations reach the western side of the ocean, the authors estimate coastal sea level by constructing a complementary coastal model. The coastal model is geostrophic and conserves mass within a nearshore region that encompasses the Gulf Stream. By extending this nearshore region as far south as 14°–18°N and using only the oceanic fluctuations to force the variability in the stream, between 80% and 90% of the variance of sea level at coastal tide gauges can be explained. Sea level along the coast is used to test the model assumptions. The basic results, however, seem important because they are constrained only by open ocean wind forcing and not by input boundary conditions.

1. Introduction

The ''rise of sea level problem'' has brought with it a whole series of unanswered questions. When we examine sea level records on the east coasts of the continents, we see surprisingly large variations at periods on the order of 100 months or longer. We are naturally led to ask what causes these variations. Do these fluctuations suggest similar changes in the transport of the western boundary currents just offshore? What is the horizontal scale of these fluctuations?

Figure 1 shows several versions of sea level on the Atlantic coast. The upper two panels show the yearly means at Fernandina and Charleston in a manner patterned after the early work of Hicks et al. (1974). A heavily smoothed version of the record at Fernandina (third panel) shows typical fluctuations greater than 10 cm, peak to peak. The final panel shows a raw periodogram (not a smoothed spectrum) at Fernandina; the spectrum is red out to periods of a few hundred months; U.S. data records are not long enough to allow very good resolution at such long periods. The records at Charleston and Fernandina, separated by only a few hundred kilometers, are ''visually coherent'' in the decadal band, but at longer distances substantial phase shifts develop and the coherence decreases irregularly.

The literature on the rise of sea level problem is extensive; see, for example, Barnett (1984), Douglas (1992), and Woodworth (1990). One of the major concerns about sea level rise is the possibility that the *rate of rise may be increasing.* The large fluctuations in Fig. 1 make it difficult to determine the rate of rise with high accuracy, so *changes* in the rate of rise will be even more difficult to discern.

This paper examines the role of wind curl variability over the open ocean as *the primary cause* of the decadal fluctuations in Fig. 1. We have shown previously (Sturges and Hong 1995; Sturges et al. 1998) that wind curl variations over the ocean can force thermocline and sea level variations that have frequencies and amplitudes similar to those of Fig. 1. Here we address the problem of how these fluctuations affect sea level at the coast.

The paper is organized as follows. After a brief description of the data sources, we briefly describe (section 3) the deep ocean part of our model, which has been explained elsewhere (Sturges et al. 1998). We then describe how the deep ocean results are used as the input

Corresponding author address: Dr. B. G. Hong, Department of Oceanography, The Florida State University, Tallahassee, FL 32306-4320.
E-mail: bg@ocean.fsu.edu

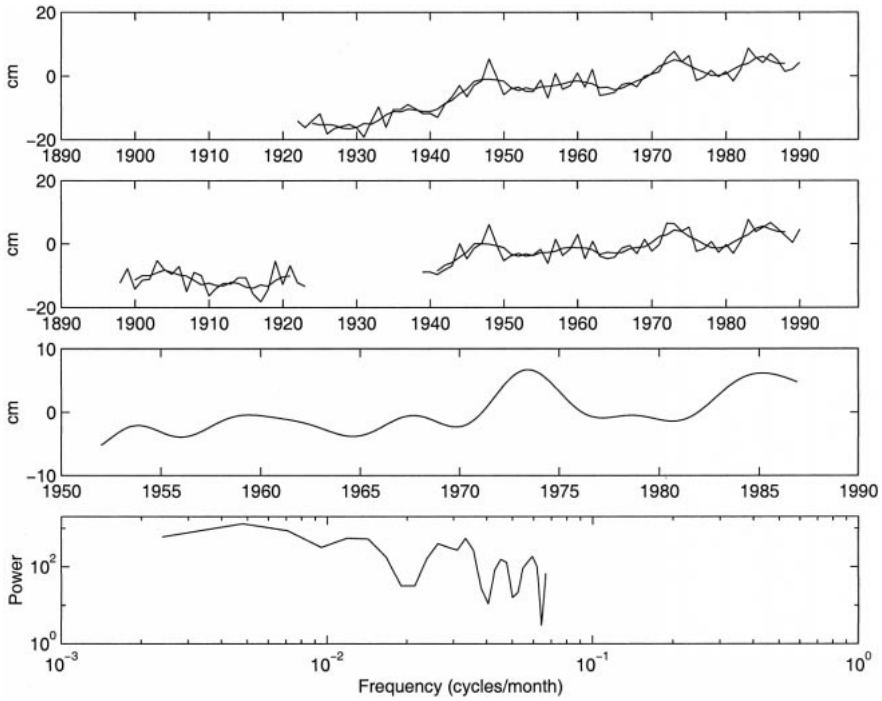

FIG. 1. The upper two panels show annual mean sea level at Charleston (32°N), South Carolina and Fernandina (30°N), Florida. The individual data points are the raw annual means and the smoothed curves are 5-yr running block averages. The third panel shows the signal at Fernandina filtered to suppress power at periods shorter than 36 months and to pass power at periods longer than 60 months. The bottom panel shows the periodogram of sea level at Fernandina at periods longer than 1 yr. A full cosine bell data window was used to reduce leakage.

to a coastal model that includes the Gulf Stream. In the results section, we approach the main result in two distinct steps. First, we make a preliminary calculation of sea level to the north of the Gulf Stream (at the Lewes, Delaware, tide gauge) using a Florida tide gauge as an input condition. It is essential to realize that this is only an intermediate step in the model's development to determine if the conceptual model has any validity. Since the model passes this test well, we then move the input boundary condition farther and farther to the south. Happily, we are able to reach a point at which there are no inputs to the model except the wind forcing, and the model output agrees with observed sea levels.

2. Data

The hydrographic data used to compute the wave speeds and vertical modal shapes were obtained from the National Oceanographic Data Center. All available hydrographic data within boxes 4° on a side were averaged to determine the properties at each grid point. These data and their distribution have been nicely described by others; see, for example, Lozier et al. (1995). In those few cases where no deep hydrographic stations were available in a 4° box, the density field was interpolated from the surrounding boxes.

We have used the Comprehensive Ocean–Atmosphere Data Set (COADS) wind dataset (see, e.g., Slutz et al. 1987). The model is forced with only the fluctuating component of the winds, after a low-pass filter is used to remove fluctuations at 3 yr and to pass those at periods of 5 yr.

Monthly mean sea level data on the U.S. East Coast are from the National Ocean Survey, NOAA. The sea level data were (in most cases) filtered in the same way as the winds to remove high frequency fluctuations. More detail is found in Sturges and Hong (1995). Some of our expanded results in movie form are also available on the World Wide Web at http://atlantic.ocean.fsu.edu.

3. The deep ocean and coastal models

a. Wind-forced deep ocean model

A simple quasigeostrophic forced long Rossby wave model of low-frequency pycnocline variability has been used here, as in our previous studies (Sturges and Hong 1995; Sturges et al. 1998), patterned after other similar studies such as those of Kessler (1990). Our model, however, is based on a separation into vertical modes. We found earlier that at the latitude of Bermuda (32°N) our results using only the first vertical mode were remarkably good and were not improved by adding higher modes. We have found here, however (as described in

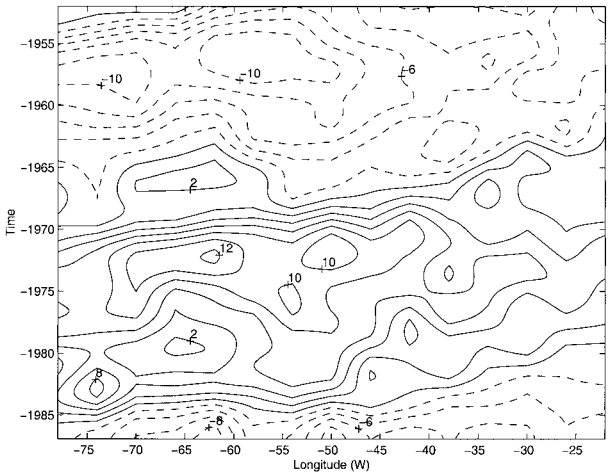

FIG. 2. Computed fluctuations in the height of sea level across the Atlantic at 18°N as functions of longitude and time. This calculation includes the first and second vertical modes. Heights are in centimeters.

a later section), that at lower latitudes the contribution of the second vertical mode improves the results substantially. The first mode speeds range from <1 cm s^{-1} in the eastern Atlantic at 38°N to >7 cm s^{-1} in the west at 18°N. Our results have not suggested any discrepancies between our computed wave speeds and the effective wave speeds in the ocean *at these latitudes and at these long periods* (see, e.g., Qui et al. 1997; Chelton and Schlax 1996).

To obtain the wind-stress curl atmospheric forcing, the monthly mean wind stresses, which are available in 2° by 2° boxes, were integrated around 4° boxes to suppress noise at the smallest scales. We have used these winds to force the model at 2° N–S resolution.

Figure 2 shows an example of the output of the model at 18°N; previously (Sturges et al. 1998, Fig 5b) we showed a similar calculation based on the first mode result alone. Here Fig. 2 shows the result from the first and second modes combined. The mean has been removed from the forcing in these examples. Figure 3 shows a snapshot example of model output for the full horizontal domain of the model. It shows a region of sea level ~4 cm high near 30°N, ~6 cm high near 22°N, and ~6 cm low in between. The essential characteristic of these figures, and of the model results, is that there tends to be a pattern, albeit a changing one, of high and low features within the subtropical gyre. There are often two highs and two lows in the north–south direction, but rarely more than one prominent high or low in the east–west direction. As these highs and lows reach the western boundary they will, of course, affect the flow, first in the Gulf Stream and then at the coast.

These fluctuations in the depth of the thermocline or in sea level are large and are wind forced. Therefore hydrographic sections in the ocean that are designed to allow calculations of oceanic flow will sometimes contain a major contribution from these signals. While this portion of the flow is ''real'' of course, it should be clear that it is strongly time dependent and not representative of the mean flow.

b. The coastal model

Our concern here is focused on the effects of these oceanic fluctuations as they are observed along the *inshore* edge of the stream. Figure 4 shows details of the area used for the ocean forcing. We also made a series of calculations (as described in the next section) extending 4° farther (to 14°N rather than stopping at 18°N), but the results were essentially unchanged.

Coastal sea level can be influenced by a number of factors, including coastal winds, river input, and offshore forcing by the deep sea. We made an extensive modeling study of the first two of these forcing mechanisms and found no agreement between observations and our calculations (appendix A describes the effort with longshore winds.). Here we report the results of forcing with the remaining candidate, deep ocean forcing.

The primary idea in our coastal model is that fluctuations in the transport of the Gulf Stream are forced along the offshore edge by the fluctuations from the open ocean. At decadal timescales, alongshore coastal flows of deep sea origin are likely to be much weaker than those over the continental slope and deep sea.

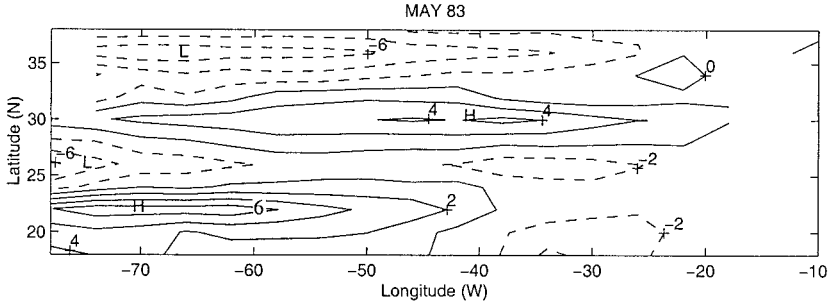

FIG. 3. An example of model output from the wind-forced model (see http://www.atlantic.ocean.fsu.edu).

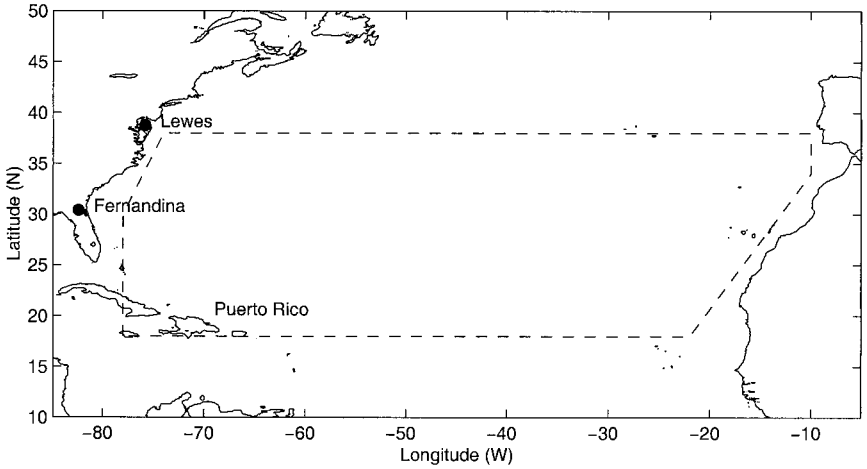

FIG. 4. Map of the model domain.

Therefore we assume that the pressure gradient across the shelf (caused by this effect) is small. This implies that coastal sea level is similar to that just seaward of the shelf edge. Thus the goal of modeling coastal sea level simplifies to modeling the shelf edge pressure.

Consider the volume V in Fig. 5 bounded at the surface by the line **AD** directly above the 100-m isobath, by the zonal lines **AB** and **DC**, and by the meridional line **BC**. The volume V is bounded below by the continental slope bottom topography when it is shallower than 1000 m; seaward of this isobath, by the horizontal plane at 1000-m depth. The sides of the volume V are vertical. The choice of 1000 m is somewhat arbitrary, although the low-frequency flow computed along **BC** has much smaller horizontal velocity at this depth than above.

The continuity equation is linear and for the low-frequency fluctuating flow can be written

$$\nabla_H \cdot \mathbf{u} + w_z = 0, \tag{1}$$

where ∇_H is the horizontal gradient operator, $\mathbf{u}$ the low-frequency horizontal velocity, w the low-frequency vertical velocity, and z the coordinate upward from the ocean surface at $z = 0$. Integrating (1) over V and using Gauss's theorem gives

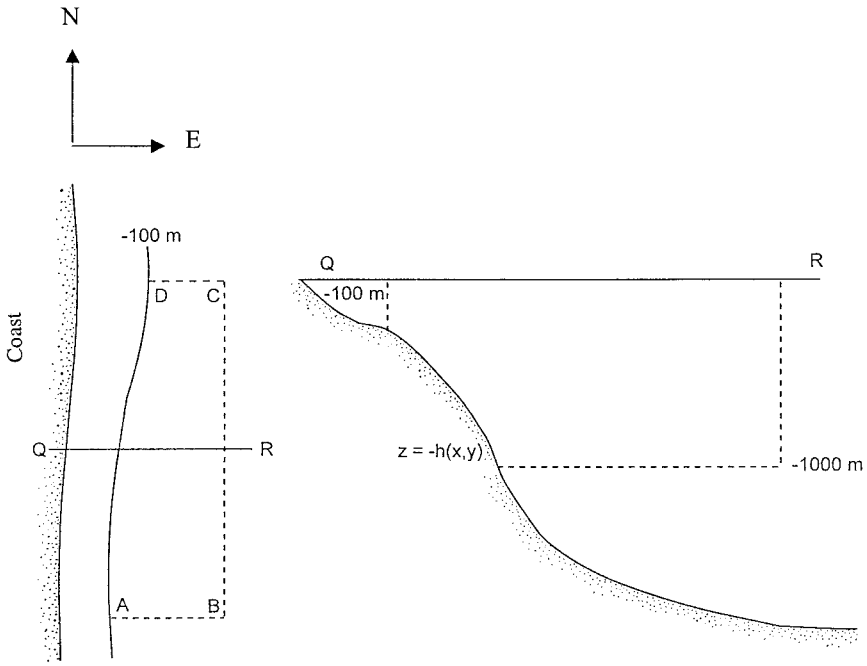

FIG. 5. Scheme of the model for sea level along the coast. The left-hand panel shows the coast at the western edge of the model; the right-hand panel shows a vertical section.

$$\int_A^D \int_{-h}^0 \mathbf{n}\cdot\mathbf{u}\, dz\, dy + \int_D^C \int_{-h}^0 v\, dz\, dx + \int_C^B \int_{-h}^0 u\, dz\, (-dy) + \int_B^A \int_{-h}^0 (-v)\, dz\, (-dx) = 0, \quad (2)$$

where **n** is the unit normal to the vertical boundary along **AD** and $h(x, y)$ is the depth of V at (x, y).

In deriving (2) we assumed that there was no flow through the surface at $z = 0$ or bottom of the volume V. There is no flow through the bottom of the control volume because there is no flow through the continental slope bottom topography; flow is also negligible through the $z = -1000$ m horizontal plane seaward of the 1000 m isobath and through the plane $z = 0$ (see appendix B).

The shelf edge depth of 100 m is shallow when compared to the main part of the volume V, so we assume that the volume transport onto the shelf is negligible compared to that across **DC**. Thus the first term in (2) is negligible, and (2) reduces to

$$\int_D^C \int_{-h}^0 v\, dz\, dx - \int_A^B \int_{-h}^0 v\, dz\, dx = T, \quad (3)$$

where T, the transport *into* the volume V, is given by

$$T = -\int_B^C \int_{-h}^0 u\, dz\, dy. \quad (4)$$

Physically, Eq. (3) states that the flow into V through **BC** is equal to the net flow out of V through **DC** and **AB**. Note that since **BC** is seaward of the western boundary flow, the linear long Rossby wave solution can be used to calculate T. It is important to note that our model calculations are for only the *fluctuating* part of the transport across **BC**.

In order to obtain simple results in terms of sea level, we assume that the surface flow is coherent in the vertical so that, for some α,

$$\int_{-h}^0 v\, dz = H\alpha v_o, \quad (5)$$

where v_o is the northward surface flow and $H = 1$ km is the depth of V seaward of the continental slope. For some constant α_N (where N specifies the northern end of the box) we may write

$$\int_D^C \int_{-h}^0 v\, dz\, dx = \alpha_N H \int_D^C v_o\, dx, \quad (6)$$

which, using the geostrophic relationship,

$$v_o = \frac{g\eta_x}{f}, \quad (7)$$

where η is the sea level at each point, reduces to

$$\int_D^C \int_{-h}^0 v\, dz\, dx = \frac{\alpha_N H g}{f_N}[\eta(C) - \eta(D)]. \quad (8)$$

A similar result holds for the southern section **AB** of V, so, in terms of sea level, (3) can be written

$$\eta(D) = \eta(C) - \frac{f_N}{\alpha_N H g}T - \frac{f_N}{f_S}\frac{\alpha_S}{\alpha_N}[\eta(B) - \eta(A)], \quad (9)$$

where the subscript S in α_S specifies the southern end of the box. In Eq. (9) the middle term involving T, the transport entering across the north–south face **BC** is determined from (4). We are able to calculate this at a resolution of 2° in the N–S direction. We know the vertical distribution of **u** from the shape of the vertical modes. North of 28°N the first mode alone is adequate because the amplitude of the second mode is negligible. South of 28°N we also include the added transport from the second vertical mode.

4. Results

a. Comparison of the deep ocean model results with observations

In a previous paper we showed (Sturges and Hong 1995) that the model output agrees with sea level at Bermuda surprisingly well. At lower latitudes we compared the model output with open ocean hydrographic data. We found (Sturges et al. 1998) that the agreement is quite good; the scatter about the best fit of <3 cm from higher-frequency motions that are not resolved is quite within the errors expected from ocean eddy motions, over a total range of ~20 cm.

Figure 6 shows a comparison between model results and a tide gauge at Magueyes Island, on the south side of Puerto Rico, near 18°N. The upper panel shows the comparison using only the first vertical mode signal; the lower panel, which also contains the second mode signal, shows not only that the agreement is better, but that it is the signals having periods of only ~5 yr that show the most noticeable improvement. These relatively shorter periods excite the second mode more effectively than the first. Because this comparison is made ''on the offshore side of the Gulf Stream,'' it is, in most respects, merely yet one more comparison similar to the initial comparison at Bermuda (as shown in Sturges and Hong 1995). The point of the comparison is that this simple model agrees reasonably well in every case where we have been able to find appropriate observations, and agreement is best at the lowest frequencies.

Figure 6 also gives an estimate of the error, or ''noise level,'' of these calculations. For the signals prior to ~1968, or during the interval ~1975–78, it is clear that an error of order 3–5 cm is common. It is only during periods of a strong signal, such as ~1972 or ~1983 that the signal emerges from the background noise. Note also that the times at which these peaks occur (i.e., the phase of the signal) will be different for different places

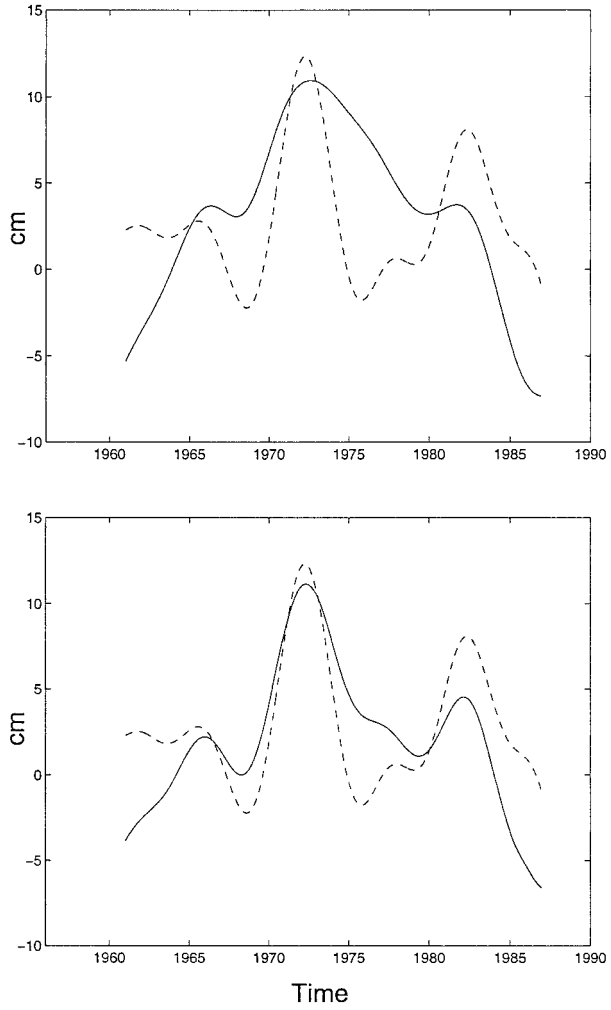

FIG. 6. Comparison between the computed result (solid line) and the tide signal (dashed line) at Magueyes Island, Puerto Rico. The upper panel shows a calculation using only the first mode, the lower panel includes first and second modes.

in the ocean; for example, the peaks occur later in Fig. 13 than here.

b. Comparing the coastal–deep sea link with observations

In order to check the link between coastal and deep sea decadal variability, we need α values for the north and south ends of the calculation in Eq. (9). If the flow were dominated by vertical mode 1, this ratio would be about 0.5. Approximately the same value is obtained by using the mean velocity measurements of Richardson et al. (1969) at a cross section near 28°N and also at a 29°N section using the mean velocity measurements of Leaman et al. (1989). Least squares fitting (9) to calculated T, $\eta(B)$, $\eta(C)$, and measured $\eta(A)$ and $\eta(D)$ also gave $\alpha \approx 0.5$. We can obtain results for ''optimized'' values of α_N and α_S (at the north and south ends of the section), but we note that these are similar to the results calculated using α from the historical mean flow results or merely using vertical mode 1. Moreover, the results are totally insensitive to the value of α_S because it eventually falls out of the calculation since far enough south the low-frequency transport through the south section **AB** (see Fig. 5) is negligible (see section 3 below). The value of α_N used in the final calculation is 0.5.

We present the results of the coastal calculations in three parts (see Fig. 7). First, we use sea level at Fernandina as an upstream boundary condition and compute sea level farther along the coast, at Lewes, Delaware. This preliminary calculation checks ''if the method works'' with our values of α_N and α_S.

The sea level fluctuations at Fernandina and Lewes are similar, so one might suspect that the use of Fernandina as an input condition is equivalent to specifying the answer. The *difference* signal between these two stations, however, has approximately the same amplitude as the signals themselves, so this is, in fact, a reasonable test of the validity of the model assumptions.

Having determined that the coastal box method produces satisfactory results, we then compute sea level at Fernandina by moving the southern boundary of the calculation farther and farther south—eventually all the way south to 14°N—where the signal from the fluctuating wind curl decreases to small values and where the effects of sea level fluctuations on the inside edge of the stream, insofar as they affect sea level farther to the north, presumably become negligible. Combining these two calculations allows computation of sea level at Lewes (and at any other location along the coast) using wind curl alone *without any observed sea level information as an input.*

1) SEA LEVEL AT LEWES, USING FERNANDINA AS AN INPUT CONDITION

Figure 8 compares observed sea level at Lewes with our model calculation. This calculation, performed as an initial diagnostic, uses sea level at Fernandina as an input boundary condition. Recall (as stated earlier) the difference signal (Lewes minus Fernandina, not shown) is as large as the signal at Lewes, so this is a valid comparison. The major peaks are modeled well; the primary quantitative comparison is to compute their cross spectra. The agreement appears to be at least as good as the accuracy of the wind field would permit. Moreover, the effect of integrating the wind signal presumably has had the effect of reducing the noise.

Figure 9 shows the cross spectra between the two results of Fig. 8. The coherence is high at the longest periods, with negligible phase shift. The coherence is also high at periods near 50–60 months, but the coherence at periods near 80 months is not quite up to the 90% confidence level. This intermediate region of frequencies having low coherence will be a consistent feature of these results. We suspect that one possible cause

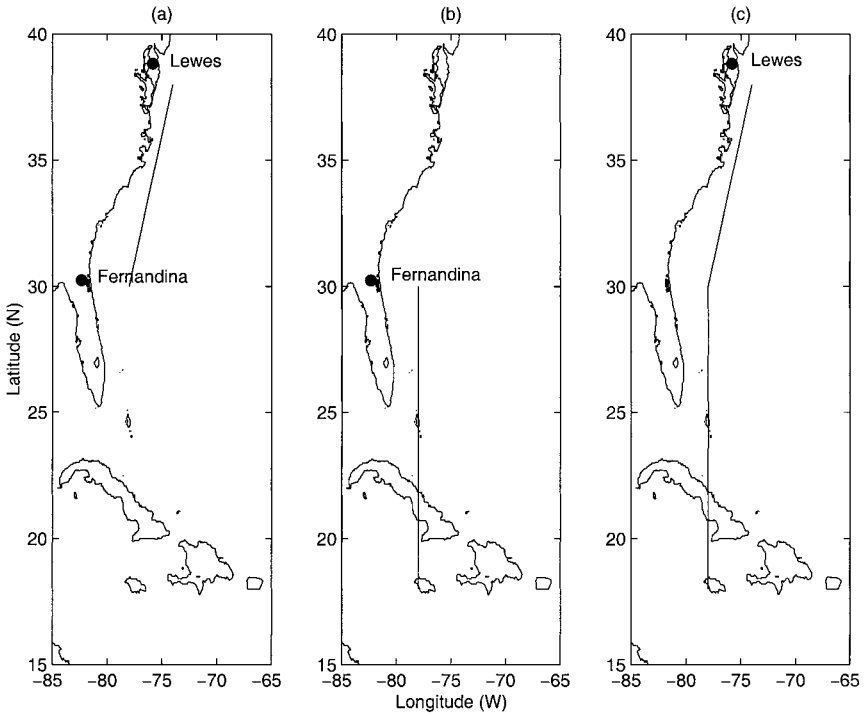

FIG. 7. A schematic showing of three different cases for the coastal model. In (a) the line offshore shows the position of the offshore boundary of the coastal box, in order to compute sea level at Lewes by using Fernandina sea level as an input condition. In (b) the line offshore shows the open ocean input region for the calculation of sea level at Fernandina. In (c) the boundary of the ocean forcing region is shown for the calculation of sea level at Lewes with no coastal input.

is a region of anomalously low power in the wind forcing, a topic treated in the discussion section.

2) SEA LEVEL AT FERNANDINA USING ONLY WIND FORCING

Because the comparison shown in Fig. 8 is encouraging, we extend the range of the wind forcing to low southern latitudes. Figure 10 shows the comparison between the model output, using only wind forcing, and observed sea level at Fernandina. For these calculations, the contributions of the first and second vertical modes are used. Figure 11 shows the cross spectra between the model output and observations. The coherence is high at the longest periods, decreasing gradually out to the limit of our frequency range. The phase shifts are small where there is appreciable power.

Figure 12 shows how much of the sea level variability can be explained as a function of the latitudinal extent of the calculation. By repeating the calculation using larger and larger north–south extents, we determined how much of the signal at Fernandina could be accounted for. Most of the variability is explained by including wind forcing to 18°N. We extended the calculation to 14°N, but this can be seen to give only a inconsequential improvement over the value at 18°N.

3) SEA LEVEL AT LEWES USING ONLY WIND FORCING

Figure 13 shows the major result of this work: a comparison at Lewes, Delaware, based on a calculation in-

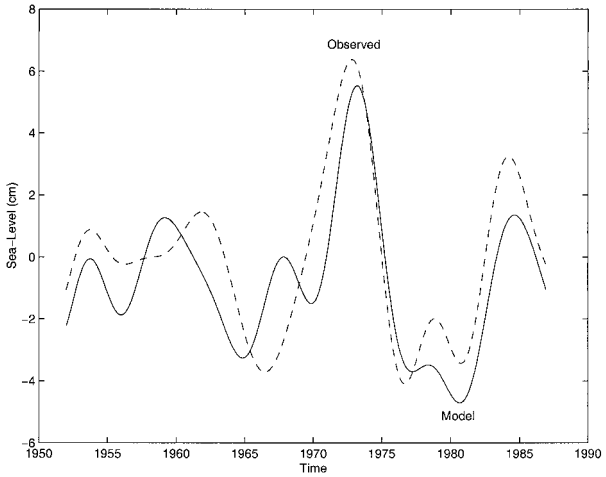

FIG. 8. Comparison between the observed sea level signal at Lewes (dashed line) and the computed result from the coastal sea level model (solid line). This result, computed largely as a diagnostic, uses sea level at Fernandina as an input to the coastal model.

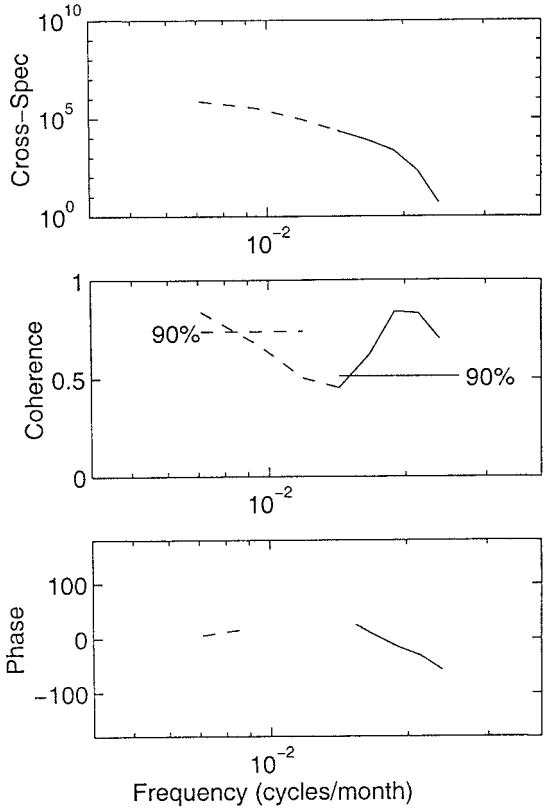

FIG. 9. Cross spectra of observed sea level at Lewes and computed signal from the model, in Fig. 8, smoothed with five-Hanning (1–2–1) passes. Dashed lines retain the next lower-frequency points using two-Hanning passes. The 90% confidence levels are shown in the coherence plot; dashed lines are for the two-Hanning result, while solid line is for the five-Hanning result. Phase is shown only when coherence squared is >90%. The confidence limits are computed as in Bloomfield (1976).

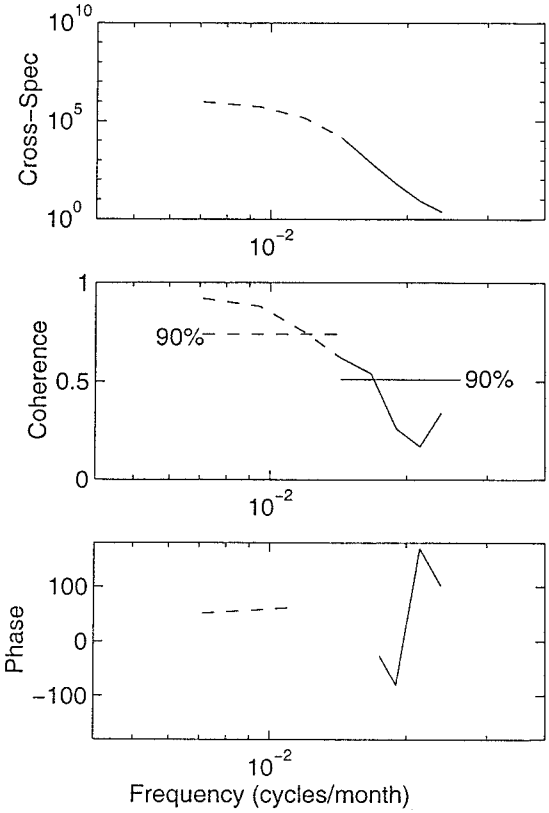

FIG. 11. Cross spectra of model and observed sea level at Fernandina, smoothed with five-Hanning passes. Dashed lines retain the next lower-frequency points using two-Hanning passes. The 90% confidence levels are shown in the coherence plot; dashed lines are for the two-Hanning result, while solid line is for the five-Hanning result. Phase is shown only when coherence squared is >90%.

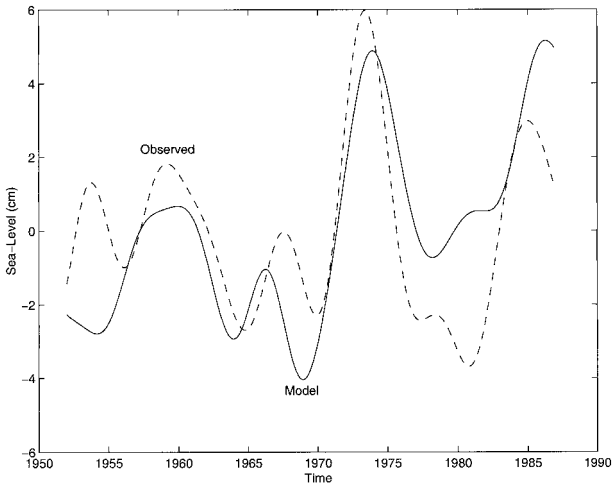

FIG. 10. Comparison between the observed sea level signal at Fernandina (dashed line) and the computed results from the coastal sea level model (solid line). No tide gauge or other observed sea level information is used to force the model in this calculation.

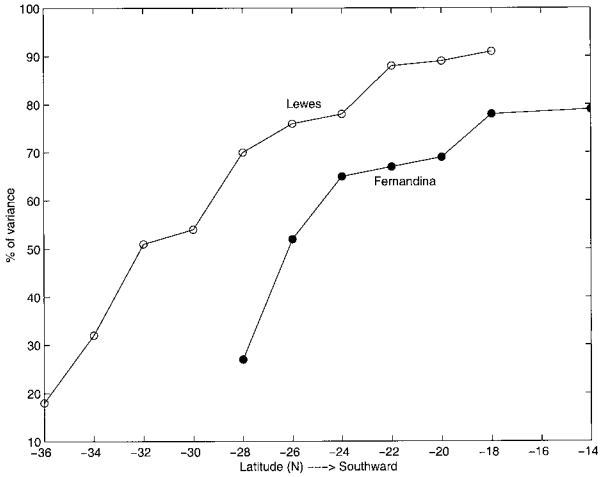

FIG. 12. Percent of variance accounted for in the computed sea level signals at Fernandina and Lewes as a function of the latitude to which the model calculations extend.

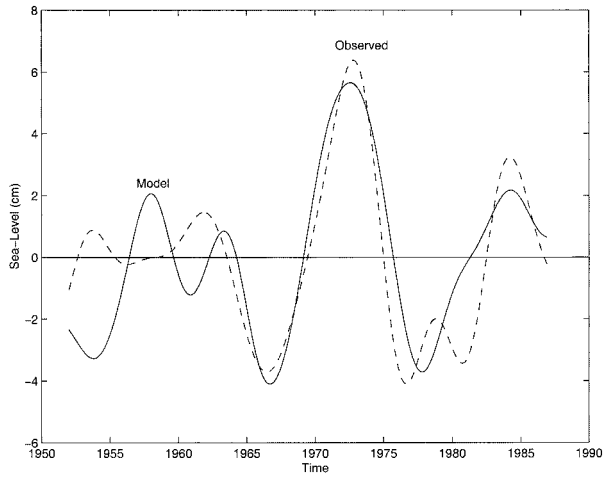

FIG. 13. Comparison between the observed sea level signal at Lewes (dashed line) and the computed result from the coastal sea level model (solid line). In this calculation no observed sea level values are used as inputs to the model.

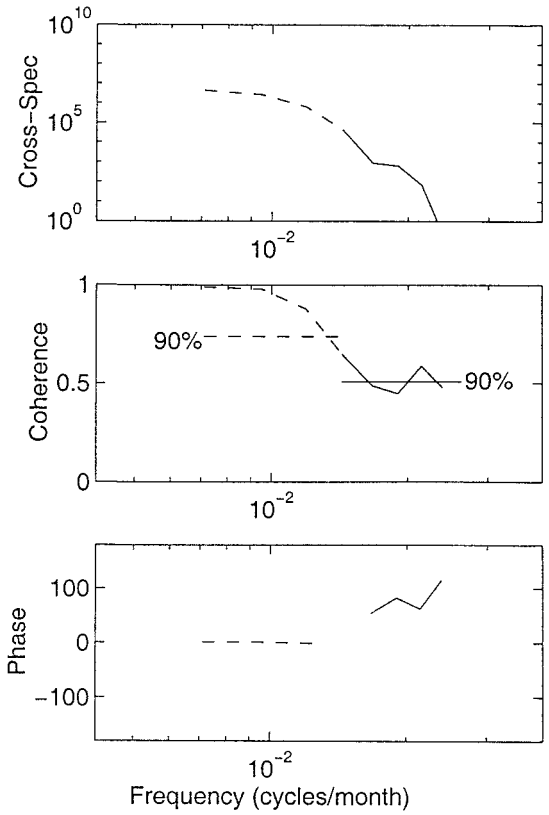

FIG. 14. Cross spectra of observed sea level at Lewes and computed signal from the model, in Fig. 13, smoothed with five-Hanning passes. Dashed lines retain the next lower-frequency points using two-Hanning passes. The 90% confidence levels are shown in the coherence plot; dashed lines are for the two-Hanning result, while solid line is for the five-Hanning result. Phase is shown only when coherence squared is >90%.

volving wind forcing alone, with no input from observed sea levels. The agreement between the two curves is quite good for the large amplitude, lowest frequency fluctuations.

Figure 14 compares the two curves of Fig. 13 in a spectral sense. As before, we find that the agreement is best at the longest periods. One might also argue that the observations of open ocean winds probably are best at the longest periods because there are more observations per cycle. The decreasing level of agreement at progressively shorter periods may represent lack of quality of the wind data, as discussed later. Figure 12 shows, as for the Fernandina result, the amount of explained variance as a function of the north–south extent of the calculation. The slope of the curve appears to decrease slightly to the south of approximately 22°–26°N as the magnitude of the curl forcing decreases. We also see that a larger fraction of the variance at Lewes is explained. Perhaps the bottom topography of the Bahamas, Cuba, and the Caribbean Islands, which our model ignores, degrades the model results at Fernandina. It is also possible that the variability from far southern forcing, which is not included here, is a larger percentage of the total signal at Fernandina.

5. Discussion

We initially attempted to model coastal variability as a result of longshore winds, as discussed in appendix A, without success. We then attempted to find convincing coherence between the observed variability and river runoff, using standard multiple input statistical models. This too proved fruitless, leaving open ocean forcing as the primary cause. Therefore, on the basis of these results, we conclude that the decadal-scale fluctuations observed at east coast tide gauges are primarily the result of variations of deep ocean wind forcing. It is essential to use the full horizontal resolution of the wind data; averaging the wind forcing destroys necessary phase information.

It is surprising that such a simple model gives a result that appears so robust. Sea level at tide gauges as well as hydrographic data in the open ocean are explained remarkably well. It is clear that, to first order, the causative mechanism is open ocean wind forcing.

This robust ocean response to noisy wind curl forcing is indicative of the basic result that, by Rossby wave dynamics, the ocean response depends on a spatial and temporal integration and therefore performs a smoothing of the wind forcing.

One puzzling feature in these results is that the coherence between observed sea level and our model calculations is high at the longest and shortest periods but is low (i.e., not above 90% confidence level) at intermediate periods. To determine if this might be related to the strength of the wind forcing, we examined the winds in some detail. Figure 15 shows the mean wind curl from the COADS dataset, averaged over the full

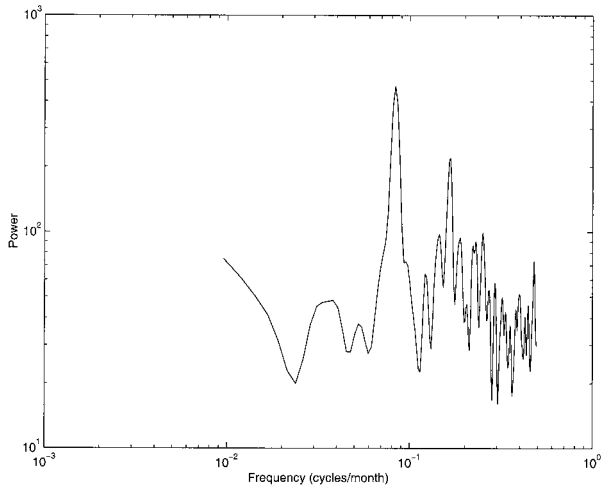

FIG. 15. Spectrum of wind curl over the North Atlantic from 18° to 38°N. A full cosine bell data window was used to reduce leakage, and the smoothing is by three Hanning passes.

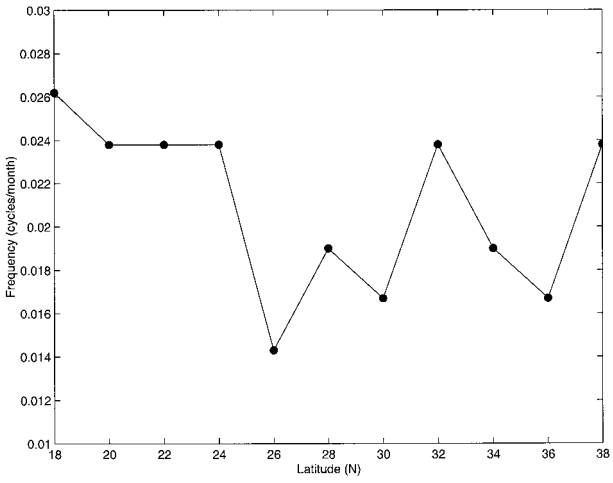

FIG. 16. The frequencies at which the low in spectral power of wind curl is found, as a function of latitude; see Fig. 15.

width of the Atlantic and for our full range of latitude (18°–38°N). (Note, however, that periods near annual and shorter were prefiltered from the winds that force the model.) The power is high at the (poorly resolved) longest periods, with a small ''bump'' of power near ~30 months, and indeed a low in spectral power at intermediate periods, similar to the low in coherence. The spectrum is shown at higher frequencies to emphasize the extent to which that power is excluded from this model. Because this feature varies geographically, Fig. 16 shows the frequency at which this low in power is observed as a function of latitude. (Such results will also depend on the time interval selected, as do all such nearly random geophysical processes.) The basic finding, however, is that the wind curl forcing at all latitudes has an intermediate region of low power, which can be ~0.014 to 0.026 cycles per month. We suggest therefore that a possible reason for the low in coherence in this intermediate frequency band between our model and observations is the result of weak wind forcing. That is, the signal-to-noise ratio is poor. It is also possible that other forcing mechanisms may be more important than wind in this intermediate frequency band.

Jin (1997) concludes that the Pacific Ocean should respond in a nearly resonant fashion to forcing near periods of 10 yr, and almost as an aside mentions that the Atlantic should respond to forcing near 5 years. However, we do not see any significant response here at periods near 5 yr (such as in Figs. 6 or 13), nor in the results of Sturges et al. (1998). One reason may be that the forcing at these periods in the COADS wind data is weak.

One other aspect of these results deserves mention. It is clear that buoyancy forcing of the open ocean is a fundamental, essential mechanism, and nothing in our results is intended to dispute its importance. Sea surface temperature variability at periods near annual is widely observed, as are long-term trends in deep-water properties well below the main thermocline (e.g., at Bermuda: S. Levitus, 1992 personal communication; Joyce and Robbins 1996). However, it appears that in the vicinity of the main subtropical gyre, for the frequency band we can resolve in this dataset, wind forcing appears to be the dominant mechanism that governs sea level variability both in the open ocean and along the east coast of the United States. It is also possible that there may be buoyancy forcing implicitly contained within the wind forcing itself, which our model does not treat explicitly and is beyond the scope of this paper.

Acknowledgments. This work was begun with support from the NOAA Office of Climate and Global Change. The recent work has been supported by the National Science Foundation, under Grants OCE-9529601 (WS) and OCE-9617304 (AJC). We thank Ms. Xiang Liu for her work with the coastal model described in appendix A. We have benefited from discussions with several of our colleagues, in particular Prof. W. Dewar and M. Stern. Dr. Steve Gill, NOAA, NOS, was particularly helpful in obtaining tide gauge data.

APPENDIX A

Estimates of Coastal Sea Level Driven by the Alongshore Wind Stress

Near the coast, at low frequencies, the cross-isobath depth-integrated transport must vanish. Under this condition, depth averaging the linearized alongshore momentum equation gives

$$0 = -g\eta_y + \frac{\tau^y}{\rho h} - \frac{\tau^y_{\text{bot}}}{\rho h}, \tag{A1}$$

where in this appendix y, g, η, τ^y, ρ, h, and τ^y_{bot} refer, respectively, to along-isobath distance, acceleration due

to gravity, sea level, along-isobath wind stress, water density, water depth, and along-isobath bottom stress. In deriving (A1) we assumed that in the water near the coast the pressure is independent of depth and that for the interannual to decadal periodicity of interest here, the time derivative term is negligible. Therefore, under the standard bottom-stress linearization

$$\tau^y_{\text{bot}} = \rho r v, \tag{A2}$$

where v is the depth averaged alongshore flow and r is a linear bottom friction coefficient, Eq. (A1) reduces to

$$\frac{rv}{h} + g\eta_y = \frac{\tau^y}{\rho h}. \tag{A3}$$

Typically on a shelf the low-frequency coastal alongshelf flow is geostrophic and highly correlated with coastal sea level. Under this scenario (A3) can be written as

$$R\eta + \eta_y = \frac{\tau^y}{\rho h g}, \tag{A4}$$

where an estimate for R is

$$R \sim r/(fhL) \tag{A5}$$

with L as the cross-shelf length scale. Typically, the length decay scale R^{-1} is approximately several hundred kilometers.

Equation (A4) is easily integrated along the coast from north to south using known coastal sea level as a starting point and either airport winds or winds from the COADS. Calculations with both sets of wind data gave similar results, suggesting that errors in wind data were small. The parameter R was varied over a wide range, including all realistic scenarios. In all cases for both wind datasets the calculated interannual to interdecadal sea level signal was unrelated to that observed. We conclude that alongshore wind forcing on the shelf is not a significant contributor to the observed interannual to interdecadal sea level signal.

APPENDIX B

Showing that the Net Vertical Flux into the Control Volume Is Negligible

First, we want to show that the flow through the horizontal plane at $z = -1000$ m at the bottom of the volume V is negligible. This will be so provided that, from Eq. (1) and (2),

$$\left|\int_P w(-H)\, dx\, dy\right| \ll \left|\int_D^C \int_{-h}^0 v\, dz\, dx\right|, \tag{B1}$$

where P is the horizontal plane of V where $z = -H = -1$ km. Advection is small at $z = -H$ and we estimate $w(-H) \sim d_t$, where d is the very low frequency isopycnal displacement. From (8) the ratio of the left-hand side to the right-hand side of (B1) is of order

$$\left|\frac{d\omega L_x L_y f_N}{\alpha_N H g[\eta(C) - \eta(D)]}\right| \approx 3 \times 10^{-2} \ll 1, \tag{B2}$$

for the reasonable values $d \approx 20$ m, $\omega \approx 2\pi/10$ yr, L_y = north–south dimension of $V \approx 2 \times 10^6$ m, $L_x \approx 2 \times 10^5$ m $\approx$ east–west dimension of V having depth H, $\eta(C) - \eta(D) = 10^{-1}$ m, $f_N = 9 \times 10^{-5}$ s^{-1}, $\alpha_N = 0.5$, $H = 1000$ m, and $g = 10$ m s^{-2}.

Second, we need to show that the flow through the plane **ABCD** (Fig. 5) at the surface $z = 0$ is negligible. This flows from an argument similar to the above with d_t replaced by

$$w|_{z=0} \sim \overline{v}\frac{\partial \eta}{\partial y}, \tag{B3}$$

where $\overline{v}$ is the mean surface flow and η is the low-frequency sea level. For $\eta \sim 10^{-1}$m and $\overline{v} = 1$ m s^{-1} we have

$$\left|\frac{\eta \overline{v} L_x f_N}{\alpha_N H g[\eta(C) - \eta(D)]}\right| \approx 4 \times 10^{-3} \ll 1. \tag{B4}$$

REFERENCES

Barnett, T. P., 1984: The estimation of ''global'' sea level change: A problem of uniqueness. *J. Geophys. Res.,* **89** (C5), 7980–7988.

Bloomfield, P., 1976: *Fourier Analysis of Time Series: An Introduction.* Wiley, 258 pp.

Chelton, D. B., and M. G. Schlax, 1996: Global observations of oceanic Rossby waves. *Science,* **272,** 234–238.

Douglas, B. C., 1992: Global sea level acceleration. *J. Geophys. Res.,* **97** (C8), 12 699–12 706.

Hicks, S. D., and J. E. Crosby, 1974: Trends and variability of yearly mean sea level 1893–1972. U.S. Dept. Commerce, NOAA, National Ocean Service, 14 pp. [Available from National Ocean Service/NOAA, 1315 East–West Highway, Silver Spring, MD 20910.]

Jin, F., 1997: A theory of interdecadal climate variability of the North Pacific ocean–atmosphere system. *J. Phys. Oceanogr.,* **27,** 1821–1835.

Joyce, T. M., and P. Robbins, 1996: The long-term hydrographic record at Bermuda. *J. Climate,* **9,** 3121–3131.

Kessler, W. S., 1990: Observations of long Rossby waves in the northern tropical Pacific. *J. Geophys. Res.,* **95** (C4), 5183–5217.

Leaman, K. D., E. Johns, and T. Rossby, 1989: The average distribution of volume transport and potential vorticity with temperature at three sections across the Gulf Stream. *J. Phys. Oceanogr.,* **19,** 36–51.

Lozier, M. S., W. B. Owens, and R. G. Curry, 1995: The climatology of the North Atlantic. *Progress in Oceanography,* Vol. 36, Pergamon, 1–44.

Qiu, B., W. Miar, and P. Müller, 1997: Propagation and decay of forced and free baroclinic Rossby waves in off-equatorial oceans. *J. Phys. Oceanogr.,* **27,** 2405–2417.

Richardson, W. S., W. J. Schmitz Jr., and P. P. Niiler, 1969: The velocity structure of the Florida Current from the Straits of Florida to Cape Fear. *Deep-Sea Res.,* **16** (Suppl.), 225–231.

Slutz, R. J., S. D. Woodruff, R. L. Jenne, and P. M. Steurer, 1987: A Comprehensive Ocean–Atmosphere Data Set. *Bull. Amer. Meteor. Soc.,* **68,** 1239–1250.

Sturges, W., and B. G. Hong, 1995: Wind forcing of the Atlantic thermocline along 32°N at low frequencies. *J. Phys. Oceanogr.,* **25,** 1706–1715.

——, ——, and A. J. Clarke, 1998: Decadal wind forcing of the North Atlantic subtropical gyre. *J. Phys. Oceanogr.,* **28,** 659–668.

Woodworth, P. L., 1990: A search for accelerations in records of European mean sea level. *Int. J. Climatol.,* **10,** 129–143.